Multiresolution Analysis on Identification and Dynamics of Clusters in a Circulating Fluidized Bed

Tung-Yu Yang and Lii-ping Leu
Dept. of Chemical Engineering, National Taiwan University, Taipei 10617, Taiwan

DOI 10.1002/aic.11758
Published online January 22, 2009 in Wiley InterScience (www.interscience.wiley.com).

A new wavelet-threshold criterion was developed to distinguish the cluster and the void phases from the transient solids holdup/concentration fluctuation signals when measured in a 108 mm-i.d. × 5.75 m-high circulating fluidized bed with FCC particles (d_p = 78 μm, ρ_p = 1,880 kg/m^3). An appropriate level of approximation subsignal was systematically specified as a threshold for cluster identification, based on multiresolution analysis (MRA) of wavelet transformation. By the established threshold, the dynamic properties of clusters including the appearance time fraction of clusters F_{cl}, average cluster duration time $\overline{\tau_{cl}}$, cluster frequency f_{cl}, and local average solids holdup in clusters $\overline{\varepsilon_{sc}}$, at different radial and axial positions were determined under the turbulent, transition and fast fluidization flow regimes. The results also describe the dynamic properties of clusters and flow patterns in the splash zone along with the dense bottom region of the circulating fluidized beds. © 2009 American Institute of Chemical Engineers *AIChE J,* 55: 612–629, 2009

Keywords: cluster identification, circulating fluidized bed, multiresolution analysis, solids holdup, wavelet transform

Introduction

The hydrodynamics and performance of circulating fluidized beds (CFBs) are often characterized by the presence of particle clusters, especially with the use of fine bed materials.[1] Over the past two decades, the study of the particle clusters has received considerable attention by experimental and numerical works in CFBs.[2–7] The dynamics of particle clusters have been found to significantly influence many important operational characteristics of CFBs, e.g., radial distribution of solid particles, heat-transfer rate, reaction kinetics, mixing of solids and gas, and pressure drop, etc.

Although there are different types of clusters existing at different positions in CFBs, i.e., streamers or strands in core and particle sheets or swarms near the bed wall region, they are usually detected as high-intensity of solids holdup/concentration fluctuation signals by fiber optic probes[2,8,9] or capacitance probes.[10–12] To quantitatively and objectively characterize the dynamic behavior of clusters from solids holdup fluctuation data, an unambiguous criterion is necessary to determine the threshold that discriminates the dense cluster phase from the continuous phase.

Soong et al.[10] proposed that general guideline for the identification of clusters: (a) the solids fraction in a cluster must be significantly above the time-average solids fraction at the same operating condition at the local position, (b) the perturbation in solids fraction, due to occurrence of cluster, must be greater than the random fluctuations in background solids fraction, and (c) the concentration increasing must be sensed for a sampling volume with characteristic length scale greater than 100 particle diameters. Based on this guideline, they defined a threshold criterion that a cluster would be identified as the transient solids holdup is greater than the time-averaged solids holdup by more than three times the standard

Correspondence concerning this article should be addressed to L-p Leu at lleulii@ntu.edu.tw.

deviation. According to Soong et al.'s[10] criterion, Tuzla et al.[11] introduced the standard that the solids holdup of a cluster must be greater than the time-averaged solids holdup by at least two times the standard deviation ($2\sigma_s$ criterion). Sharma et al.[12] also modified Soong et al.'s[10] criterion and proposed a mean-referenced criterion. They introduced the concept that the starting time of a cluster is the last time its density/solids holdup exceeds mean density/solids holdup $\bar{\varepsilon_s}$ before satisfying the $2\sigma_s$ criterion, and the ending time of a cluster is the first the density/solids holdup falls below $\bar{\varepsilon_s}$, after falling below the $2\sigma_s$ limit.

Independent researchers (Manyele et al.[9] and Liu et al.[13]) recently considered that the coefficient n of σ_s is not unique with respect to Soong et al.'s[10] criterion, and should be estimated systematically by quantitative analysis under different operating conditions including superficial gas velocity, solid mass flux, axial levels and radial position of riser bed. Manyele et al.[9] proposed a sensitivity analysis to identify the optimal threshold of solids concentration. They introduced the cluster time fraction as a sample parameter, and obtained a sharp change as the coefficient n of σ_s increases beyond the optimal value that demarcates the particulate and the cluster phases. In addition, they stated that the optimal n varies with the solid-mass flux; hence, different n values should be applied for different operating conditions. Liu et al.[13] characterized the particle clustering behaviors by the phase Doppler particle analyzer (PDPA) measurement and proposed a semi-empirical method to identify the optimal coefficient n. They plotted the cluster occurrence frequency as a function of n for some typical operating conditions, and examined the optimal value of n by the overlap of the first plateau of all the curves in the plots. However, the aforementioned studies based on Soong et al.'s[10] criterion were called into question by Guenther and Breault.[14] They asserted that the identification criterion of clusters based on the mean and standard deviation was statistically meaningless, because the optic fiber signal in this case is not normally distributed and non-stationary. The fiftieth percentile of their fiber optic data is suggested as the threshold to identify the particle clusters.

So far, a clear-cut definition or satisfactory criterion of cluster identification is still lacking especially for FCC particles in the dense bottom region of CFBs. A proposed criterion should be able to precisely characterize the properties of particle clusters, and also be physically meaningful. In addition, the gas-solids flow in CFB systems usually exhibits time-variant, multiscale and nonlinear dynamic behaviors conduced by the chaotic interaction between the void and the solids (dense cluster) phases.[7,15–17] These behaviors are always reflected by the fluctuations of solids holdup data. Employing the time-averaged parameters, i.e., mean and standard deviation, as the threshold criterion for cluster identification might neglect the time-variant, multiscale and nonlinear components of solids holdup fluctuations. It eventually leads to the wrong estimation of cluster dynamic properties. Hence, an analytic method taking readings of the aforementioned considerations should be adopted for cluster identification from the transient solids holdup fluctuation signals.

Wavelet analysis is a powerful tool for signal processing, and has been widely applied in various scientific and engineering fields over the last decade. It is especially applicable in dealing with time-variant signals comprising nonlinear and multiscale features. In recent years, several studies have applied wavelet analysis to characterize the dynamic behaviors of clusters in fluidized beds. The first study of wavelet analysis on the time series of solids holdup was proposed by Ren and Li[18] who decomposed the solids holdup signals into three scales of components: microscale, mesoscale and macroscale, which correspond to the particle, cluster and equipment size, respectively. Ren et al.[19] proposed a principal component method, deduced by the wavelet spectrum function, for phase separation from the solids holdup signals in a 90-mm-i.d. CFB with FCC particles. They separated the dense cluster phase (cluster scale), and dilute phase (particle scale) from original solids holdup signals, based on the maximum scale parameter of wavelet spectrum function, however, no further discussion on cluster properties was presented. Ellis et al.[20] carried out wavelet transform on the voidage fluctuation data at the bubbling and turbulent flow regimes. They determined skewness and kurtosis of detail and approximation subsignals to characterize the motions of voids and dispersed particles in different wavelet scales. Wang et al.[7] specified the flow patterns of clusters and the dispersed particles in a riser by positive and negative peaks of the detail signals from wavelet multiresolution analysis of the simulated particle concentration fluctuations. Lu et al.[21] also determined the cluster frequency and size by the cross-correlation and wavelet analysis of local voidage signals in a downer CFB. Guenther and Breault[14] analyzed the fiber optic signals by using discrete wavelet analysis to characterize the dynamic behavior of clusters of cork particles at different axial and radial positions in a large scale CFB operated at three different flow regimes. They proposed two rules of wavelet analysis to determine the length and count of clusters based on the 50th percentile value of the reconstructed signal.

In this study, a wavelet-threshold criterion was established by means of multiresolution analysis (MRA) of wavelet transform that made it possible to distinguish the dense-cluster phase from the gas-void phase for FCC particles. In addition, by this criterion an attempt was also made to determine the dynamic properties of clusters at different radial positions in the splash zone and the dense bottom region, in order to gain deeper insight about the dynamic behaviors of clusters in a laboratory-scaled CFB unit.

Experimental

Experiments were carried out in a circulating fluidized bed of 108 mm-i.d.×5.75 m-high as shown schematically in Figure 1. It is a transparent Plexiglas column equipped with a loop-seal type nonmechanical valve for returning the entrained particles. An expanded top section made of stainless steel is 1.5 m in height, with five times the cross-sectional area of riser bed as employed by Shou and Leu.[22] A perforated plate, distributed with 250 holes of 1.5-mm dia., giving an open-area ratio of 4.8 % is used as the gas distributor. Ambient air is supplied by a Roots blower to fluidize the particles. The spent FCC particles with an average particle size of 78 μm, and particle density of 1880 kg/m^3 are used as the bed material. The static bed height of the bed material is 0.6 m. The minimum fluidization velocity estimated based on Wen and Yu[23] is 4.5×10^{-3} m/s. The transition velocities U_c and U_k, characterized by the standard

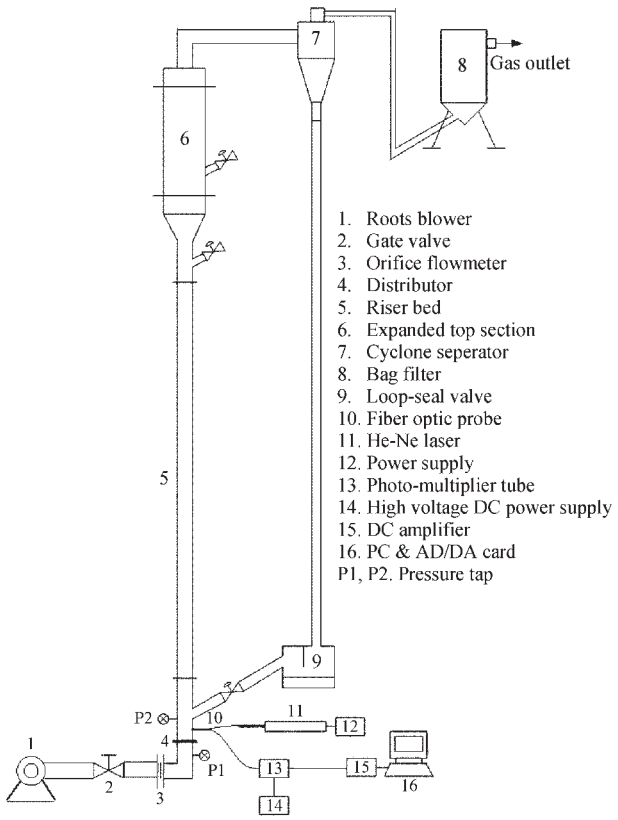

Figure 1. Experimental setup.

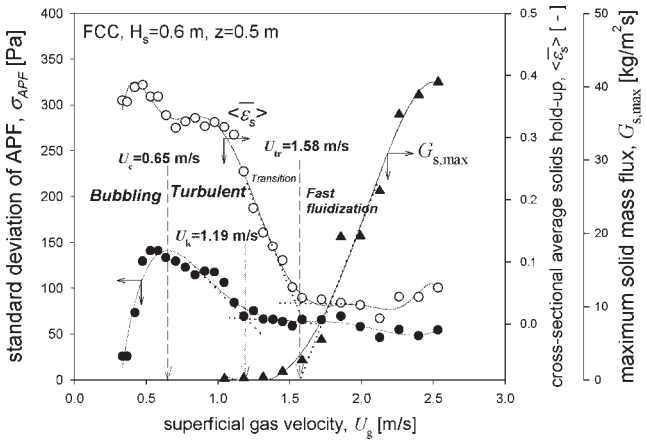

Figure 2. Standard deviation of APF, cross-sectional average solids holdup and maximum solid mass flux vs. the superficial gas velocity.

deviation of pressure fluctuations, are 0.65 and 1.19 m/s, respectively, as shown in Figure 2. The transport velocity U_{tr}, obtained from the maximum G_s vs. U_g (proposed by Schnitzlein and Weinstein[24]) is 1.58 m/s, which coincided well with the blowout velocity U_{se}, as predicted by Bi et al.[25] Based on the transition velocities U_c, U_k and U_{tr}, three superficial gas velocities of 0.91, 1.45, and 1.86 m/s are taken to investigate the cluster dynamics in the turbulent, transition and fast fluidization flow regimes, respectively. The solids holdup measurements were carried out at six radial positions from the bed wall to the bed center (r/R = 1, 0.8, 0.6, 0.4, 0.2 and 0) in the dense bottom region (z = 0.5 m), and the splash zone/transition region (z = 1.15 m) of the riser bed. For each run of experiments, the solids holdup fluctuation signals were acquired by a reflective-type fiber optic probe and recorded by an AD/DA card at a sampling rate of 10^3 Hz, with a total sampling time of 24.6 s. Multiresolution analysis (MRA) of wavelet transformation on the solids holdup fluctuation signals were performed by a wavelet toolkit of S-PLUS software (MathSoft, Inc.).

Calibration of fiber optic probe

A reflective-type fiber optic probe composing of plastic fibers of 1-mm and 500-μm dia., similar to the probe D introduced by Ishida and Tanaka,[26] was used to measure the transient solids holdup fluctuation signals in the circulating-fluidized bed. The dimensions of the probe are shown in Figure 3. A calibration procedure proposed by Zhang et al.[27] was carried out. The calibration apparatus which mainly consisted of a controllable solids feeding system, a 16.6 mm-i.d.$\times$0.4 m-long test pipe and a shutter valve, as shown in Figure 4, was used. First, the fiber optic probe was installed on the wall of the test pipe between the two slide plates of the shutter valve. FCC particles dropping from the storage tank through the test pipe were stably provided by regulating the vibrator or replacing the orifice with different open areas to keep particles flowing through the pipe with different solids holdups. When FCC particles passed the tip of fiber optic probe, the receiving optical fiber transmitted the reflective

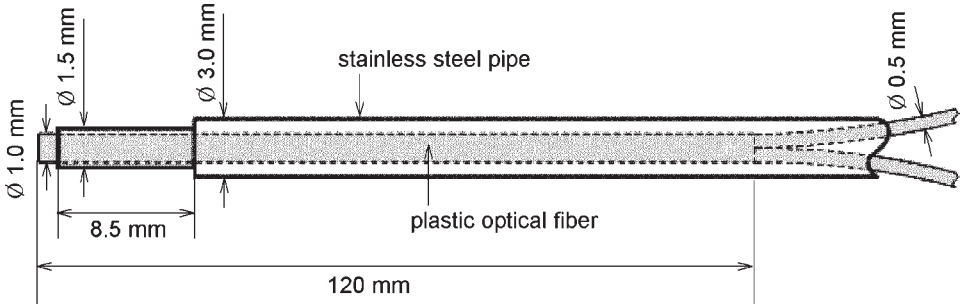

Figure 3. Schematic diagram of the fiber optic probe.

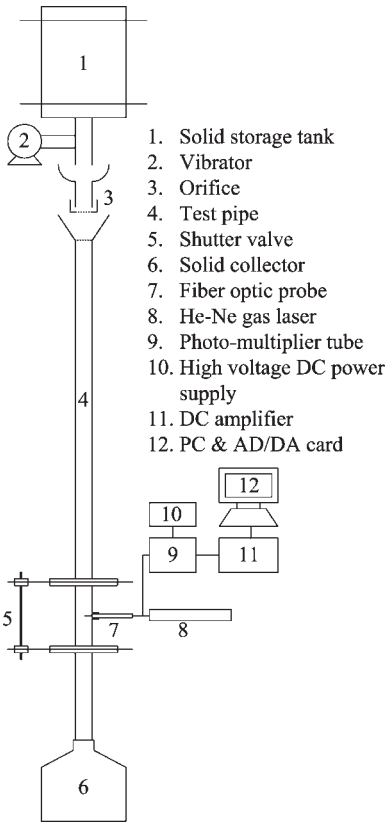

Figure 4. Calibration system of the fiber optic probe.

light from the surface of FCC particles to a photomultiplier. As the fiber-optic signal data were logged into a personal computer via an AD/DA card, the shutter valve was closed in a very short time period. Thus, FCC particles were immediately trapped in the test pipe between the two slide plates of the shutter valve, and were taken out to be weighed. Then the solids holdup was able to be determined by the following relationship

$$\overline{\varepsilon_s} = \frac{m}{S\,\Delta L\,\rho_{\mathrm{p}}} \tag{1}$$

where m is the mass of FCC particles captured in length ΔL between the two slide plates of the shutter valve; S is the cross-sectional area of the test pipe.

To make sure the different measurements are made on the same basis, the intensity of reflective light should be normalized as follows (Herbert et al.[28])

$$\bar{I} = \frac{I_1 - I_0}{I_{\max} - I_0} \tag{2}$$

where I_1 is the intensity of measured reflective light at any condition; I_0 is the intensity of light in empty bed, and $I_{\max}$ is the intensity of reflective light in loosely packed bed. By linear regression of $\bar{I}$ and $\bar{\varepsilon_s}$ in logarithmic coordinates, two correlations for FCC particles in the dilute ($0 < \bar{\varepsilon_s} \leq 0.0266$) and dense ($0.0266 < \bar{\varepsilon_s} \leq 0.545$) flow conditions were obtained as shown in Figure 5.

Data Processing

Wavelet theory

Wavelet analysis was used for transforming the transient solids holdup fluctuation signals in this study. Similar to a windowed Fourier transform, a wavelet transform can measure the time-frequency variations of spectral components, while providing more flexible time-frequency resolutions. The transform on a discrete signal can be carried out by discrete wavelet transform (DWT). The essence of DWT is to expand a signal, $x(t)$ ($t = 1, \ldots, N$), as a sum of base functions $\phi_{j,k}(t)$ and $\psi_{j,k}(t)$ produced by dilations and translations of the orthogonal father wavelet function ϕ, and the mother wavelet function ψ shown as follows

$$\phi_{j,k}(t) = 2^{-j/2}\phi\left(\frac{t - 2^j k}{2^j}\right) \quad j,k \in I \tag{3}$$

$$\psi_{j,k}(t) = 2^{-j/2}\psi\left(\frac{t - 2^j k}{2^j}\right) \quad j,k \in I \tag{4}$$

where $k = 1, 2, \ldots, N/2^j$ is the time shift and $j = 1, 2, \ldots, J$ is the transformed level. J is the maximum level of wavelet transform and is dependent on ϕ, ψ and N. Thus, the wavelet transform of $x(t)$ can be obtained by Eq. 5 and Eq. 6

$$a_{J,k} = \int x(t)\phi_{J,k}(t)dt \tag{5}$$

$$d_{j,k} = \int x(t)\psi_{j,k}(t)dt \tag{6}$$

where $a_{J,k}$ and $d_{j,k}$ are called the approximation and detail coefficients, respectively. Roughly speaking, $a_{J,k}$ mainly represents the smooth/low-frequency behavior of $x(t)$ at the coarser scale, and $d_{j,k}$ represents the detail/high-frequency part at the finer scale.

Multiresolution analysis developed by Mallat[29] can be applied to decompose the signal $x(t)$ into orthogonal signal components of hierarchical scale. The approximation subsignal $A_J(t)$, and the detail subsignal $D_j(t)$, which represent the components of $x(t)$ at different resolutions, are calculated as follows

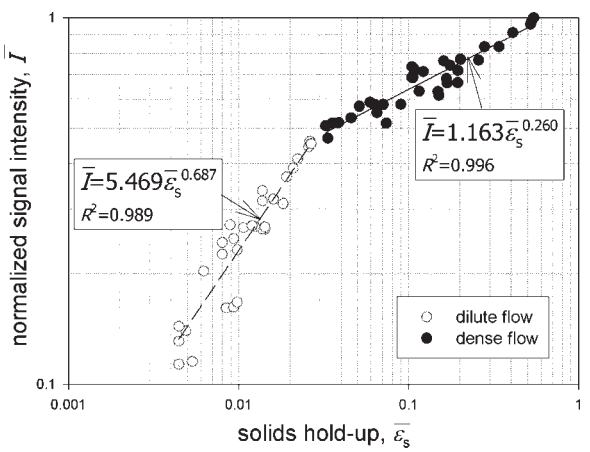

Figure 5. Relationship between the normalized intensity of reflective light and the solids holdup.

Table 1. The Approximate Frequency Bands of the Detail and Approximation Subsignals Based on the Sampling Frequency of this Study

	Approximation frequency band [Hz] (for $f_s=10^3$ Hz)	
Level j	Approximation A_j(t)	Detail D_j(t)
1	0−250	250−500
2	0−125	125−250
3	0−62.5	62.5−125
4	0−31.3	31.3−62.5
5	0−15.6	15.6−31.3
6	0−7.81	7.81−15.6
7	0−3.91	3.91−7.81
8	0−1.95	1.95−3.91
9	0−0.977	0.977−1.95
10	0−0.488	0.488−0.977
11	0−0.244	0.244−0.488
12	0−0.122	0.122−0.244
13	0−0.0610	0.0610−0.122

$$A_J(\mathrm{t}) = \sum_k a_{J,k}\phi_{J,k}(\mathrm{t}) \quad J,k \in \mathrm{I} \tag{7}$$

$$D_j(\mathrm{t}) = \sum_k d_{j,k}\psi_{j,k}(\mathrm{t}) \quad j,k \in \mathrm{I} \tag{8}$$

D_j(t) contains an approximate frequency band of $[f_s/2^{j+1}$–$f_s/2^j]$ Hz and A_J(t) contains an approximate frequency band of $[0$–$f_s/2^{J+1}]$ Hz. Here f_s is the sampling frequency and 2^j is the scale factor at level j. The ranges of approximate frequency band of D_j(t) and A_j(t), based on the sampling frequency (f_s = 10^3 Hz) in this study were summarized in Table 1. Based on the two-scale correlation of wavelet function, the approximate frequency bandwidth and center frequency of D_j(t) are half those of D_{j-1}(t), as well as A_j(t) against A_{j-1}(t).

Consequently, the finer scales of D_j(t) mainly capture the detail/high-frequency feature of x(t), while the larger scales of D_j(t) and A_j(t) mainly reveal the whole-view/low-frequency feature of x(t). By MRA, the signal x(t) is hierarchically decomposed into a series of D_j(t) and A_J(t); inversely, it also can be reconstructed from D_j(t) and A_J(t) by the inverse discrete wavelet transform (IDWT) algorithm. The decomposition and reconstruction/synthesis processes are schematically shown in Figure 6.

The energy of A_J(t) and D_j(t) are defined as follows

$$E_J^A = \sum_{\mathrm{t}=1}^{\mathrm{N}} |A_J(\mathrm{t})|^2 \tag{9}$$

$$E_j^D = \sum_{\mathrm{t}=1}^{\mathrm{N}} |D_j(\mathrm{t})|^2 \tag{10}$$

Based on the orthogonality and the energy conservation of MRA, the total energy of x(t), E, can be calculated by the sum of E_j^D (j = 1, 2, …, J) and E_j^A as follows

$$E = \sum_t |x(\mathrm{t})|^2 = E_J^A + \sum_{j=1}^{J} E_j^D \tag{11}$$

Because of good localization and extremely small error of reconstruction (the relative error is smaller than 10^{-15}), the third-order Daubechies' wavelet (Daublet3) is used to carry-out MRA on the solids holdup fluctuation signals in this study.

Calculation of dynamic properties of clusters

Dynamic properties of clusters determined in this study included the appearance time fraction of clusters F_{cl}, average cluster duration time $\overline{\tau_{cl}}$, cluster frequency f_{cl}, and local average solids holdup in clusters $\overline{\varepsilon_{sc}}$. The definitions of these properties similarly used by Sharma et al.[12] are given as follows:

- Appearance time fraction of clusters F_{cl}: the fraction of total time when clusters exist at the sampling volume of probe. This is calculated by the ratio of total cluster duration time to total sampling time T

$$F_{cl} = \frac{\sum_{i=1}^{n_{cl}} \tau_i}{\mathrm{T}} \tag{12}$$

where τ_i = $\mathrm{t_b}$-$\mathrm{t_a}$ is the time length of the ith cluster, as depicted between 4 and 5 s at the abscissa in Figure 9d. It is calculated from the product of the sampling time interval (1/f_s), and the counts of data point above the threshold value between t_a and t_b.

- Average cluster duration time $\overline{\tau_{cl}}$: total cluster duration time averaged by total number of clusters n_{cl} in a sampling time. n_{cl} is equal to the number of peaks above the corresponding threshold values and is determined by a built-in program of LabVIEW software (National Instrument Co.) in this study

$$\overline{\tau_{cl}} = \frac{\sum_{i=1}^{n_{cl}} \tau_i}{n_{cl}} \tag{13}$$

- Cluster frequency f_{cl}: the average number of clusters identified per second during total sampling time

$$f_{cl} = n_{cl}/\mathrm{T} \tag{14}$$

- Local average solids holdup in clusters $\overline{\varepsilon_{sc}}$: since the distribution of solids fraction in clusters is approximately a Gaussian type[30] $\overline{\varepsilon_{sc}}$ can be determined by integrating sampled solids holdup values of each cluster $\overline{\varepsilon_{sc,i}}$, and averaged by total number of clusters detected

$$\overline{\varepsilon_{sc}} = \frac{\sum_{i=1}^{n_{cl}} \overline{\varepsilon_{sc,i}}}{n_{cl}} \tag{15}$$

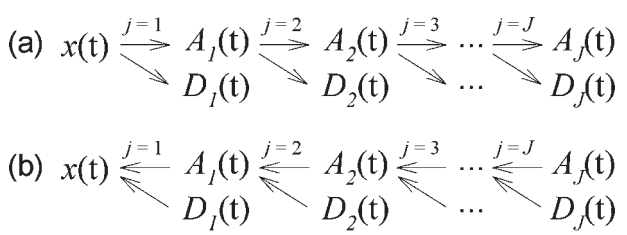

Figure 6. Multiresolution analysis for (a) signal decomposition, and (b) signal reconstruction.

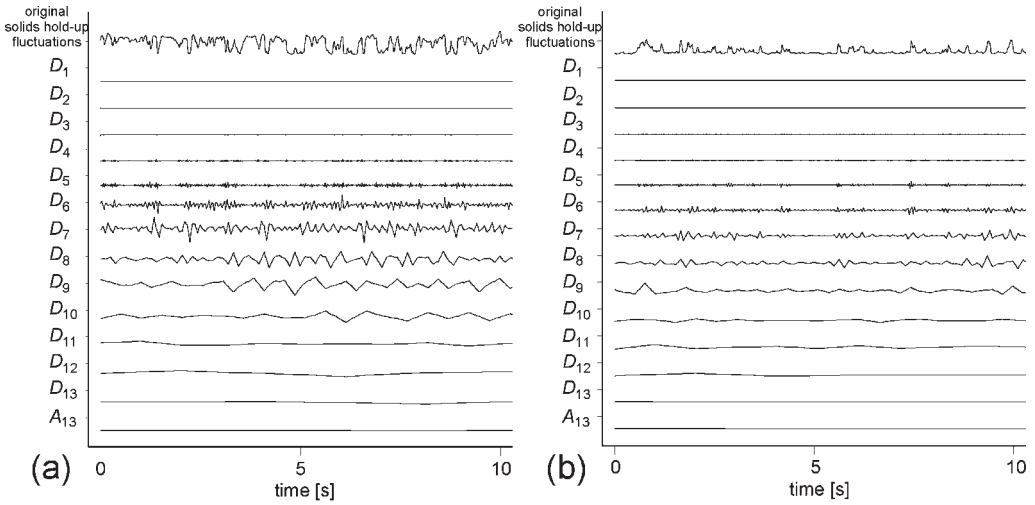

Figure 7. MRA of solids holdup fluctuation signals at (a) z = 0.50 m, and (b) z = 1.15 m (U_g = 0.91 m/s, G_s = 0 kg/m^{2}s, r/R = 0.6).

Results and Discussion

Cluster identification

Cluster identification was systematically performed by MRA on the solids holdup fluctuation signals in this study. We developed an alternative procedure to determine the threshold for solids holdup which delineated the transition between the dense cluster and the gas void phases. The procedure is introduced as follows.

First, a transient solids holdup fluctuation signal was decomposed into D_1, D_2, ..., D_{13} and A_{13} subsignals by the decomposition procedure of MRA (the maximum level J of decomposition was determined by the number of sampling points N). As shown in Figure 7, the multiscale behaviors of the original solids fluctuation signals were presented along the evolution of time.

Second, the energy of each level of subsignal was calculated by Eqs. 9 and 10. Figure 8 shows the normalized wavelet energy distribution describing the contribution of each level of subsignal involved in the original solids holdup fluctuation signal. As demonstrated by Ren and Li,[18] the multiscale behaviors exhibited in a fluidized bed lead to multiple components in the original solids concentration signals. They are recognized as three scales: microscale (particle size), mesoscale (cluster size), and macroscale (equipment size). These three scales were also discriminated from the energy distribution in Figure 8. Subsignals D_1–D_4 of small scale/high frequency mainly originated from noise or individual particles passing the probe tip in both gas void and dense cluster phases. Subsignals D_5–D_{11}, referred to as mesoscale, mainly captured the dynamics of clusters. They contained most of the energy of the original signal. Ren et al.[19] stated that if the size of the probe is in the same order of magnitude as clusters, the predominant scale in the original signal should contain the information of cluster behavior. The residual subsignals D_{12}, D_{13} and A_{13} originating from the background fluctuations of the entire CFB system were referred to as macroscale, which oscillated at a frequency lower than 0.25 Hz. Hence, a threshold separating the cluster scale from the background unit scale might be between the dominant scale and the largest scale in Figure 8.

Third, A_{13} and D_{13} were synthesized to yield the finer scale approximation subsignal A_{12}. Continuously, A_{12} was taken to be synthesized with D_{12} to yield the approximation subsignal A_{11}. This reconstruction process was repeated until the dominant level $j = 8$ was approached, in the same way, the approximation subsignals from A_8 to A_{13} were obtained. Figure 9a–f show the approximation subsignals from A_8 to A_{13} plotted with the original solids holdup fluctuation signal in a segment of sampling period. The relatively larger peaks in the original solids holdup signal mainly represented the appearance of particle clusters with higher solids holdup near the probe tip. The approximation subsignals of different levels j characterized the variation of the original solids holdup signal in different time scales 2^j or frequency bands. With decreasing the level of approximation subsignal from $j = 13$ to 8, the amplitude of approximation subsignal A_j became larger and most of the large peaks in the original solids holdup signal was eventually covered by A_j as like A_8 shown in Figure 9a. On the contrary, when the level increased, the approximation subsignal became smoother and eventually

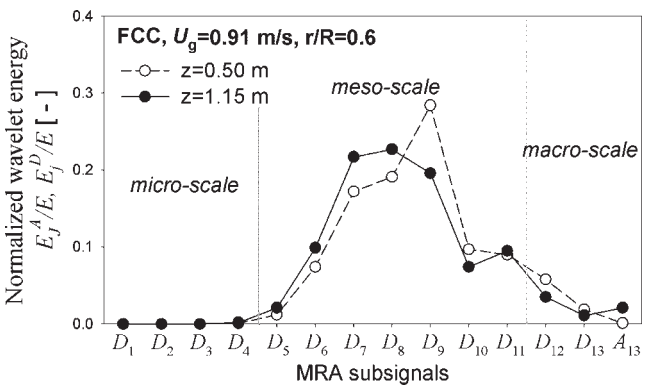

Figure 8. Normalized wavelet energy distribution.

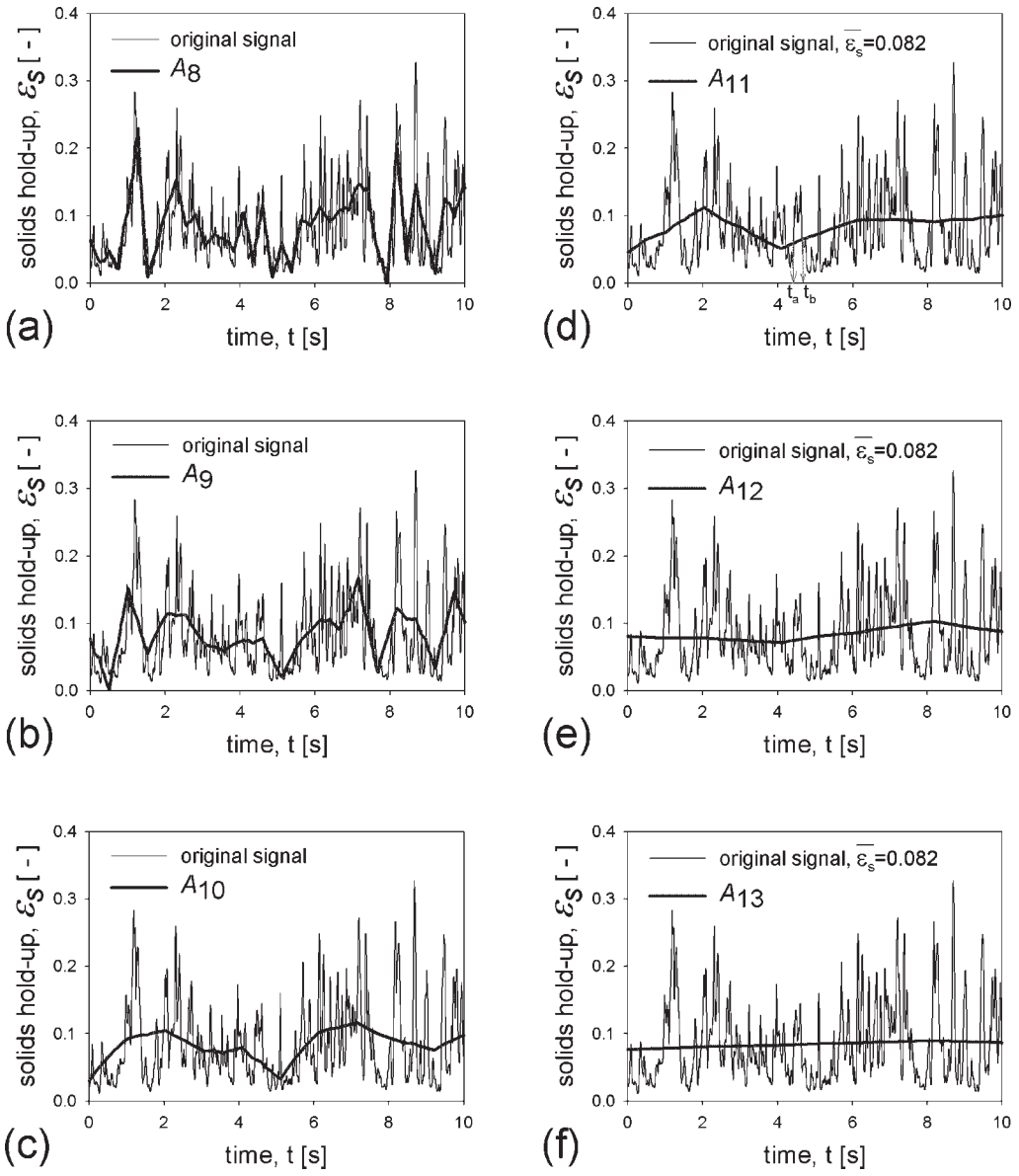

Figure 9. Fluctuations of the original solids holdup signal, and the approximation subsignals of (a) A_8, (b) A_9, (c) A_{10}, (d) A_{11}, (e) A_{12} and (f) A_{13}.

approached the mean value of the original solids holdup fluctuation signal, as A_{12} or A_{13} shown in Figure 9e or 9f. If A_8 was used as a threshold for cluster identification, most of the peaks (clusters) in the original solids holdup fluctuation signal were filtered out. This was because many peaks in A_8 vs. time curve almost overlapped the peaks in the original solids holdup fluctuation signal, e.g., the large peak between the time 0.75 and 1.50 s in Figure 9a. However, if an approximation subsignal with larger time scale, like A_{12} or A_{13}, was specified as a threshold, the time-variant feature of original solids holdup fluctuation signal would be ignored. For example, the original solids holdup at the time from $t = 0$ to 1 s and from $t = 3$ to 5 s was lower than that at other moments, but no clear trend could be observed from A_{12} or A_{13}. A detailed description of different levels of approximation subsignals for cluster identification is shown in the Appendix.

According to the earlier discussion, an approximation subsignal of a suitable level considered as the threshold should not only identify most of the clusters, but also characterize the time-variant features of the original solids holdup fluctuation signal. Once the appropriate level was specified, clusters could be directly identified from the peaks, which had higher solids holdup than the threshold value. However, the main problem this study would like to address is which level of the approximation subsignal should be taken as the threshold for cluster identification, and whether it is suitable for the solids holdup signals measured from other conditions (flow regimes, radial and axial positions in bed). These problems were required to have been resolved prior to the following investigations of the cluster dynamic behaviors.

To decide which level of the approximation subsignal was adopted as a threshold, the relationships between the cluster

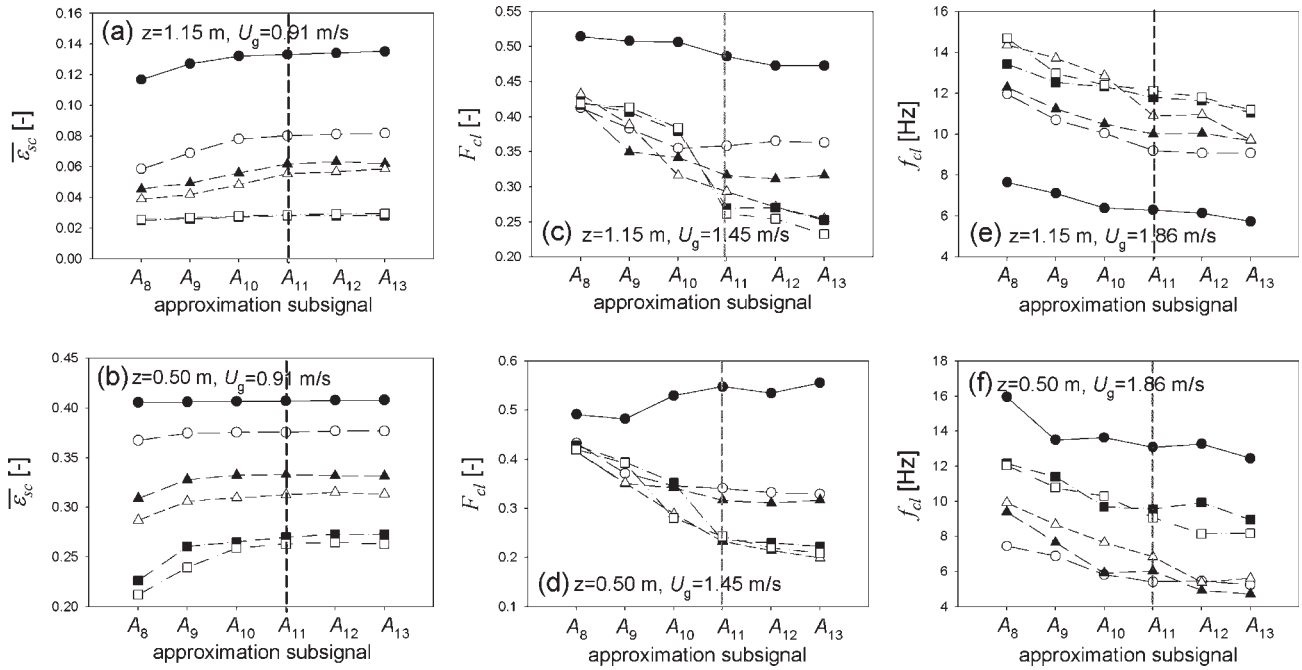

Figure 10. Dynamic properties of clusters vs. the approximation subsignals of different levels.

(●: r/R = 1.0, ○: r/R = 0.8, ▲: r/R = 0.6, △: r/R = 0.4, ■: r/R = 0.2, □: r/R = 0).

dynamic properties ($\overline{\varepsilon_{sc}}$, F_{cl} and f_{cl}), and the approximation subsignals of different levels (from A_8 to A_{13}) at different radial positions were investigated under various experimental conditions, as shown in Figure 10a–f. These figures indicated that the dynamic properties of clusters were more or less affected by the level of approximation subsignals. With the increase of the level, the average solids holdup in clusters $\overline{\varepsilon_{sc}}$ gradually increased to relatively higher values and kept almost constant beyond level $j = 11$, as shown in Figure 10a and b. The appearance time fraction F_{cl}, and the frequency of clusters f_{cl} attenuated with the increase of the level, and also began to level-off at level $j = 11$, as shown in Figure 10c–f. Besides, the difference of cluster properties determined by another approximation subsignal adjacent to A_{11}, i.e., A_{10} or A_{12}, was quite small with the relative error of less than 10 %. Recalling the discussion in the last paragraph, an approximation subsignal with too large or too small scale would somewhat lose the time-variant feature of original solids holdup fluctuation signals or the dynamics behavior of clusters, respectively. Hence, the approximation subsignal A_{11} was a compromise choice as the threshold for cluster identification from the solids holdup fluctuation signals. It comprised the fluctuations with a period of $2^{11}/f_s$ (f_s is the sampling frequency), and also operated similar to the moving-averaged line of the original solids holdup fluctuation signals. A cluster was then identified when the transient solids holdup exceeded the value of A_{11}; it existed until the solids holdup once again dropped below the value of A_{11}. Based on the approximation subsignal A_{11}, the dynamic properties of clusters, consequently, could be determined by Eqs. 12–15.

Recently, Guenther and Breault[14] investigated cluster length and count of cork particles by wavelet analysis. They took the 50th percentile value of reconstructed solids holdup signal as the threshold for cluster identification. Their threshold criterion was also applied to our experimental data, and compared with the wavelet A_{11}-threshold here. As shown in Figure 11, both of the thresholds could identify particle clusters from the distinct peaks in the original solids holdup fluctuation signal. It was found that the wavelet A_{11}-thershold had the intensity of solids holdup quite close to the 50th percentile threshold (see the middle row plots of Figure 11), and nearly no obvious difference was observed in the cluster phase fluctuations for both thresholds (see the bottom row plots of Figure 11). The dynamic properties of clusters obtained by these two thresholds are shown in Figure 12. It reveals that both thresholds generated similar radial cluster distribution for the four dynamic properties. Furthermore, the difference of F_{cl} determined by the two thresholds was not significant, as well as f_{cl} and $\overline{\tau_{cl}}$; $\overline{\varepsilon_{sc}}$ based on the two thresholds being almost the same. The slight difference could be ascribed to the fact that the 50th percentile threshold was a constant value, while the wavelet A_{11}-thershold was not, which tracked the time-variant features of the original solids holdup fluctuation signals.

Figures 13 and 14 show the global view of original solids holdup fluctuation signals and the corresponding wavelet A_{11}-threshold (represented by a dashed line) at different radial positions in the dense bottom region and splash zone of the bed. Both figures clearly showed that at constant U_g, the intensity of wavelet A_{11}-threshold increased when increasing the relative radial distance from the center of the bed, as

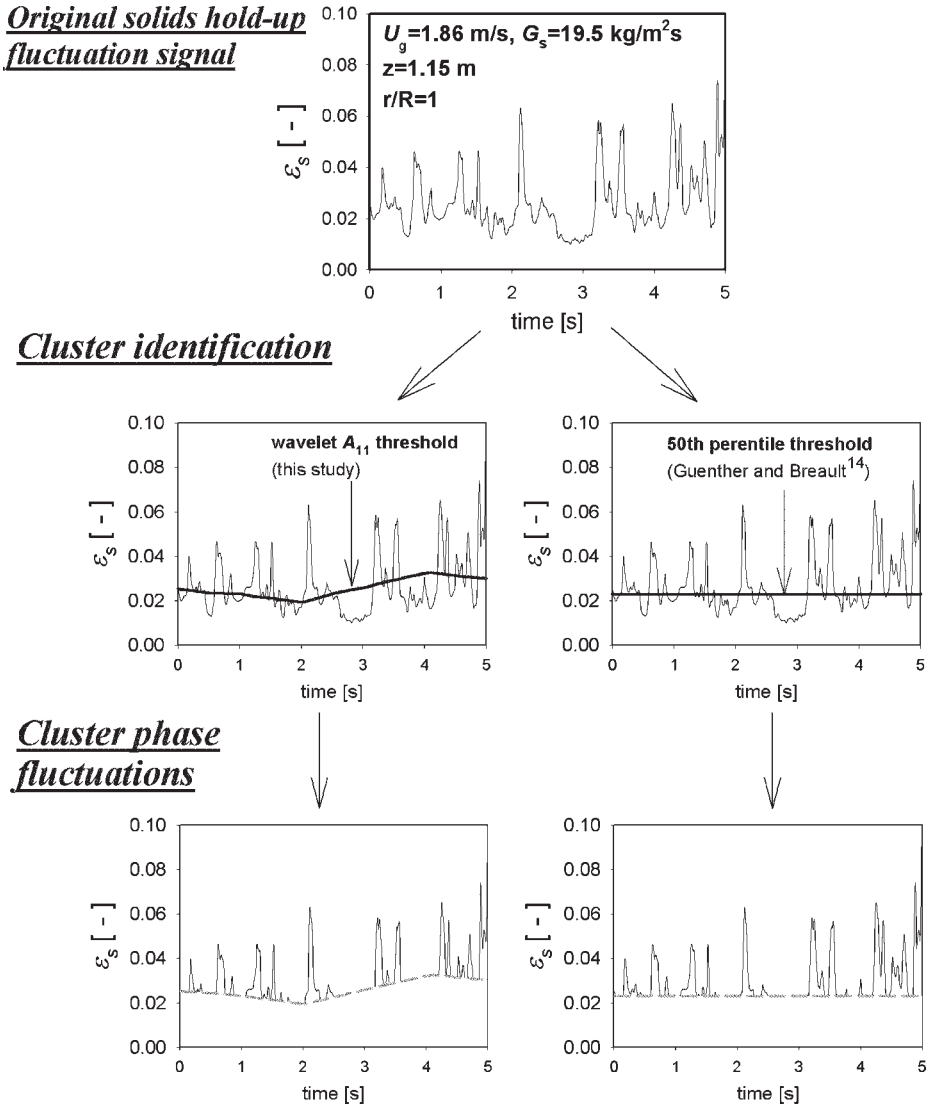

Figure 11. Cluster identification by using the wavelet A_{11}-threshold and 50th percentile threshold.

well as the corresponding original solids holdup fluctuation signal. In addition, the wavelet A_{11}-threshold captured the global tendency of original solids holdup fluctuation signal, and simultaneously separated the cluster phase (large peaks) from the background dilute phase (small fluctuations with low solids holdup).

In the dense bottom region (Figure 13), a great quantity of large peaks, corresponding to the particle clusters with higher solids holdup, was clearly observed in the turbulent flow regime (U_g = 0.91 m/s, G_s = 0 kg/m^{2}s). As U_g increased, the particle clusters became sparser and their solids holdup became more diluted in the transition and fast fluidization flow regimes. At higher elevation (Figure 14), the particle clusters in the core of the bed were rarer than those near the bed wall in both the turbulent and the transition flow regimes. Besides, the particle clusters in the transition flow regime had somewhat higher solids holdup than in the turbulent flow regime, especially near the bed wall. This was because in the turbulent flow regime, most solid particles kept in the dense bottom region, while in the transition flow regime, significant amount of solid particles in the dense bottom region was entrained to the splash zone by higher gas velocity. Some of those entrained solid particles tended to aggregate into larger clusters and then fell downward near the bed wall. When U_g further increased over the transport velocity of particles, the aforementioned phenomenon became more and more significant. The solids holdup in clusters near the bed wall was even one-order higher than that near the core region of bed, as revealed in the subplot at the bottom row of Figure 14.

Probability density function (PDF) analysis

Probability density function (PDF) analysis mainly provides information about the frequency count of the number of times that a specified interval occurs in a sequence. To get more clear understanding of the cluster phase structures in the lower portion of the riser for different operating condi-

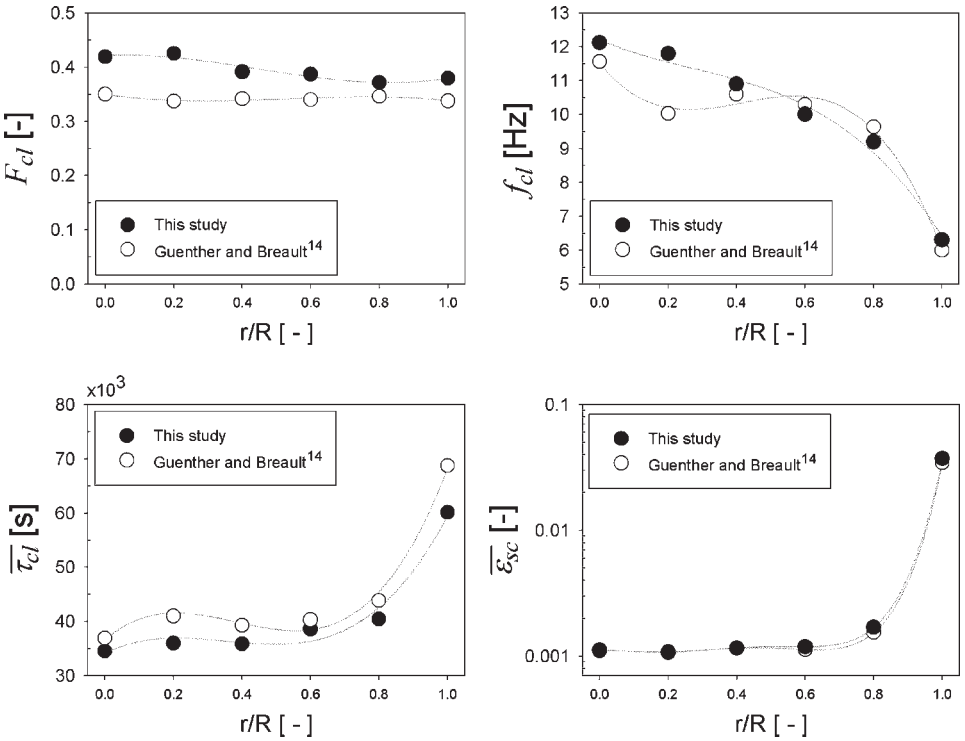

Figure 12. Comparison of cluster dynamic properties determined by the wavelet A_{11}-threshold and 50th percentile threshold.

tions, PDF of the original solids holdup fluctuation signal (the solid line), PDF of wavelet A_{11}-threshold (the short-dashed line), PDF of the solids holdup in the dense cluster phase (the dot-dashed line), and the median (or the 50th percentile) of the corresponding solids holdup fluctuation signal (the vertical straight line) are shown in Figure 15. In the splash zone of the riser (z = 1.15 m), PDF of original solids holdup fluctuation signal revealed a unimodal distribution without obvious change when the flow regime varied from the turbulent to the transition flow regime (Figures 15a and b). However, it quickly shifted to very narrow solids holdup distribution when the flow regime transformed from the transition to the fast fluidization flow regime (Figure 15c). PDF of the dense cluster phase first displayed a similar unimodal

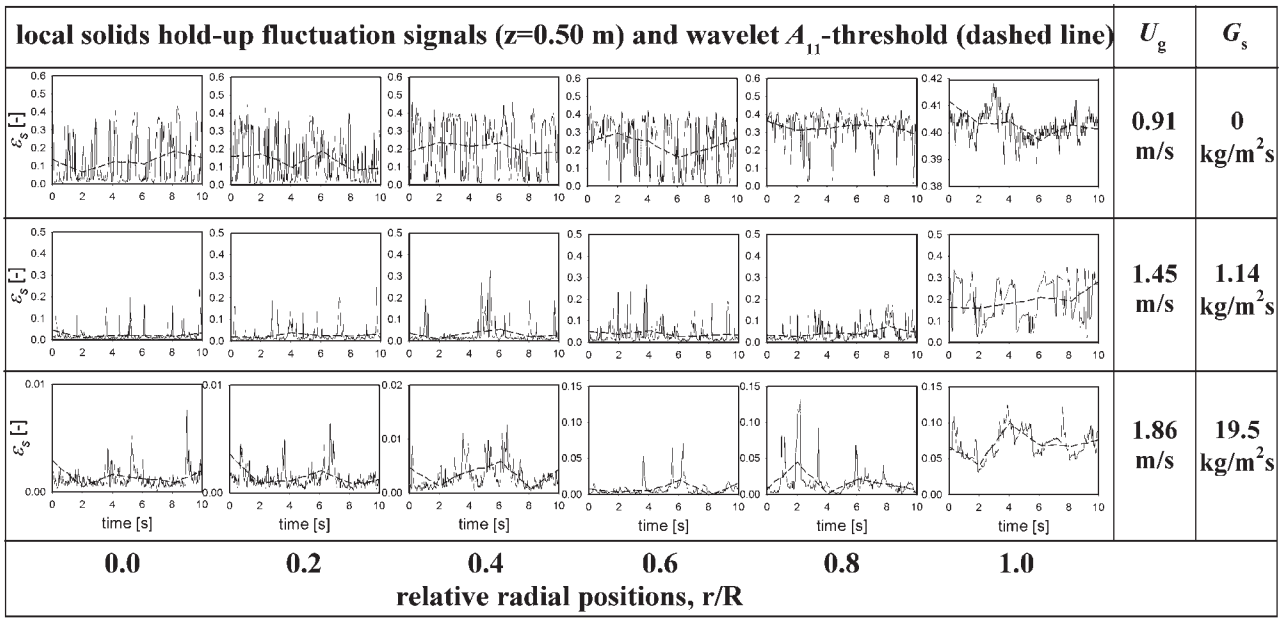

Figure 13. Cluster identification by the wavelet A_{11}-threshold at various experimental conditions for z = 0.50 m.

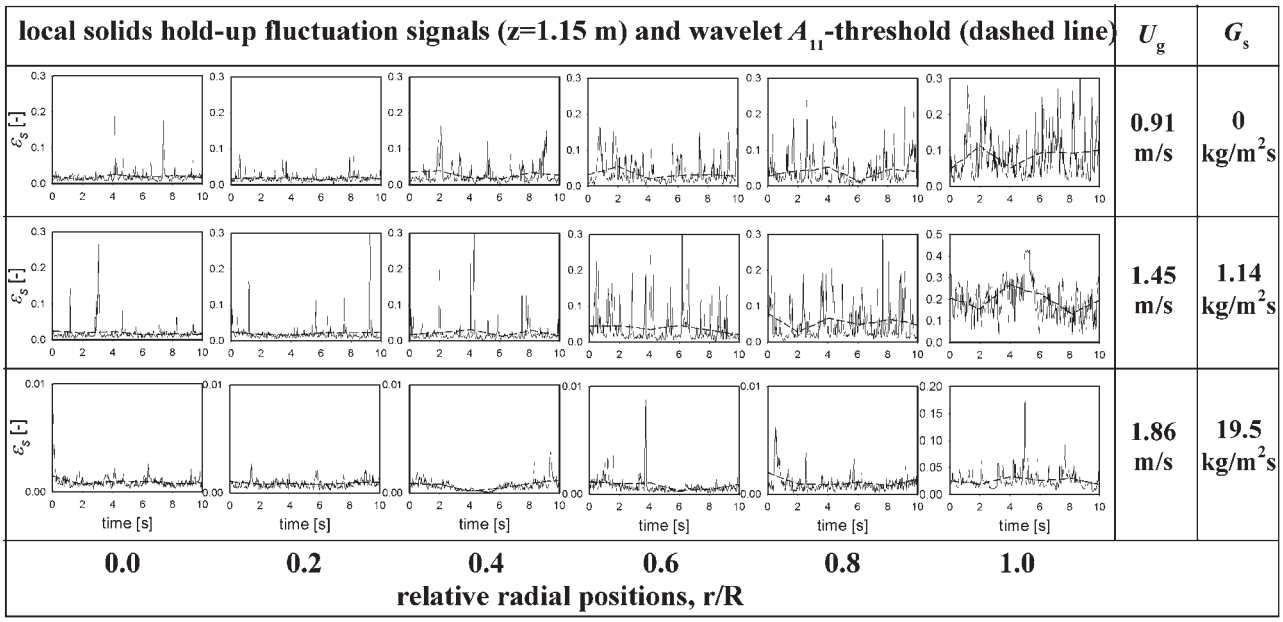

Figure 14. Cluster identification by the wavelet A_{11}-threshold at various experimental conditions for z = 1.15 m.

distribution as that of original fluctuations in the turbulent flow regime (Figure 15a), while a distinct peak appeared near the median in the transition flow regime (Figure 15b). This might be ascribed to the acceleration of clusters associated with enlarged dilute cloud structure around the clusters. When U_g further increased, the difference between the solids holdup in the dense cluster phase, and in the surrounding cloud phase gradually reduced because of the increase of shear force acting on them; eventually, the coexistence of these phases disappeared. Therefore, PDF of dense cluster phase again formed in a unimodal distribution in the fast fluidization flow regime, as shown in Figure 15c. In addition, both the solids holdup of the original fluctuation signal and the dense cluster phase in this flow regime had much lower value (<0.003) than those in the transition flow regime. This implies that both the dense-cluster phase and the surrounding gas void phase became more dilute in the fast fluidization flow regime. Comparing the PDFs of the dense cluster phase in the splash zone, a unimodal distribution with its tail biasing to higher solids holdup could be observed both in the tur-

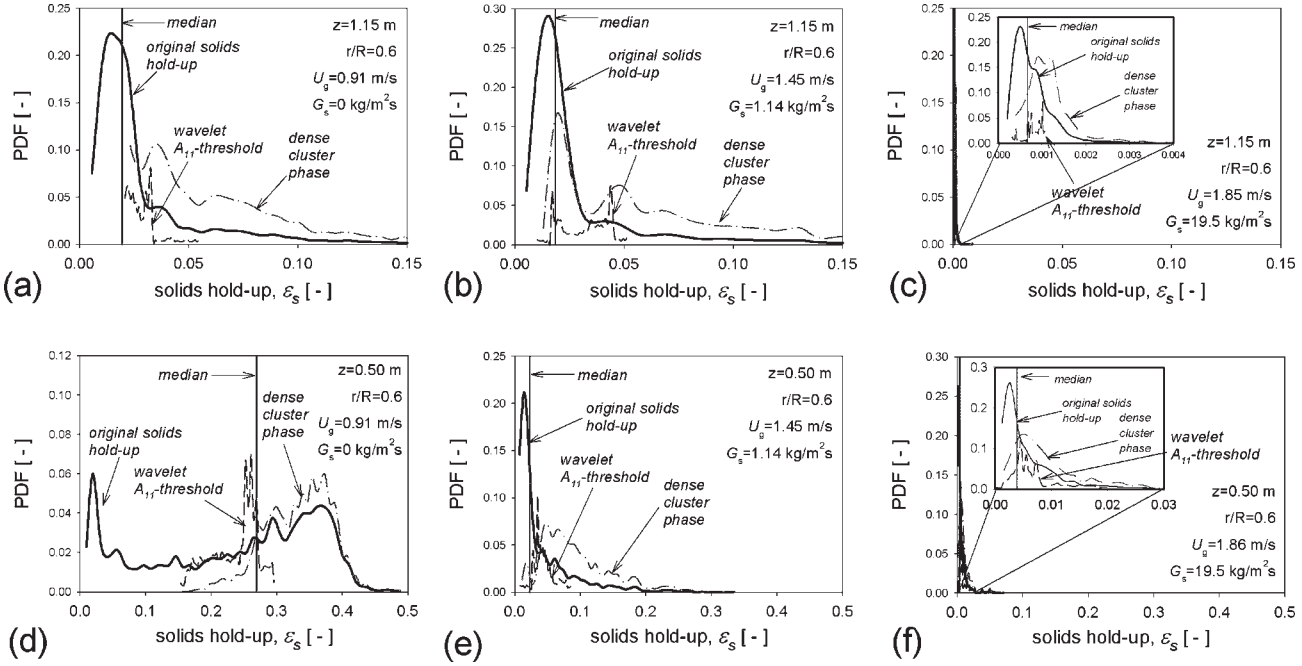

Figure 15. Probability density function of original solids holdup —, the dense-cluster phase – · –, and the wavelet A_{11}-threshold ----.

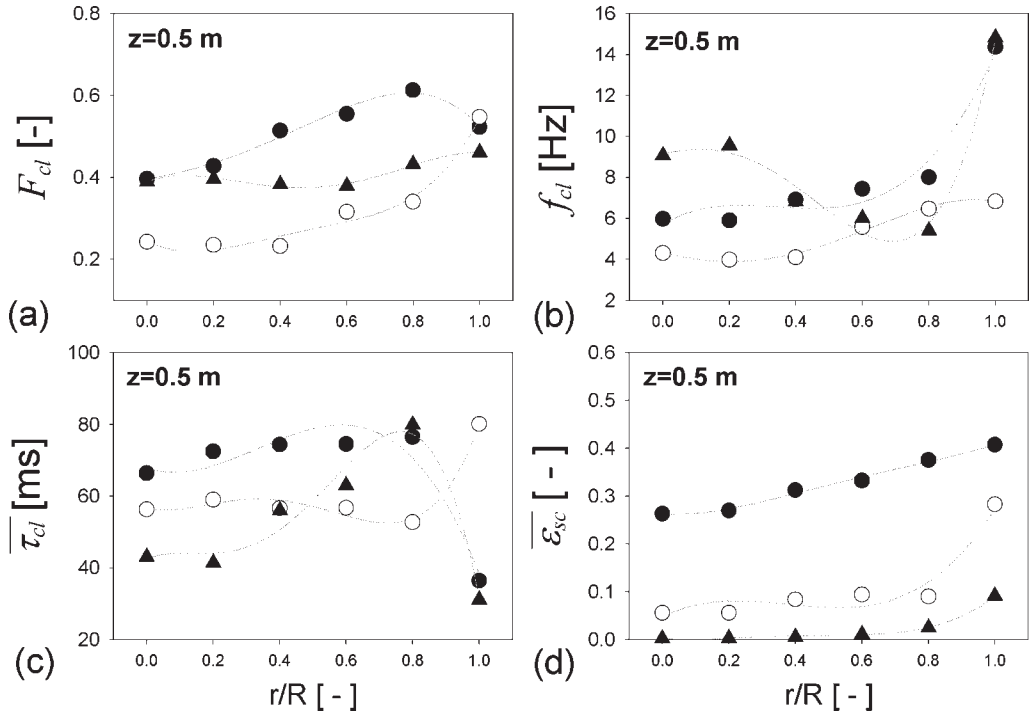

Figure 16. Radial distribution of dynamic properties of clusters in the dense-bottom region (z = 0.5 m).

(●: U_g = 0.91 m/s, G_s = 0 kg/m^{2}s; ○: U_g =1.45 m/s, G_s = 1.14 kg/m^{2}s; ▲: U_g = 1.86 m/s, G_s = 19.5 kg/m^{2}s).

bulent and the fast fluidization flow regimes, while the solids holdup of dense cluster phase in the turbulent flow regime ($0.02 < \varepsilon_s < 0.164$) was significantly higher than that in the fast fluidization flow regime ($3.88 \times 10^{-4} < \varepsilon_s < 3.44 \times 10^{-3}$).

In the dense bottom region of the riser (z = 0.5 m), PDF of the original solids holdup fluctuation signals showed a clear bimodal distribution in the turbulent flow regime (Figure 15d); this was also observed by other authors.[30–32] It gradually changed to the unimodal distribution as the gas velocity increased (Figure 15e and f). PDF of the dense cluster phase having the unimodal distribution quickly biased from the righthand side to the lefthand side when the gas velocity increased. This implies that the solids holdup in the dense cluster phase was significantly affected by the operation conditions, and the effect was apparently more pronounced than that in the splash zone. For PDF of wavelet A_{11}-threshold, there was no clear rule of dependency with the increase of gas velocity. However, we found that PDF of A_{11} was mainly distributed around the median value, and showed similar bias as that of the original solids holdup fluctuation signal in each plot. This result implies that the wavelet A_{11}-threshold was suitable for cluster identification by analyzing the solids holdup fluctuation signals, which were usually not normally distributed.

Radial distribution of cluster dynamic properties

Radial distribution of dynamic properties of clusters in the dense bottom region (z = 0.5 m), and in the splash zone (z = 1.15 m) were determined based on the wavelet A_{11}-threshold, as shown in Figures 16 and 17. They will be discussed in this section individually.

Appearance time fraction of clusters F_{cl}

In the dense bottom region (z = 0.5 m), the radial distribution of F_{cl} was relatively higher near the bed wall, and gradually decreased toward the core region as the riser was operated in the turbulent flow regime (Figure 16a). When the flow regime changed to the transition state by increasing U_g, F_{cl} at all radial positions (except near the bed wall) apparently became lower due to the significant number of FCC particles in the dense bottom region injected into the splash zone. However, F_{cl} became slightly higher again, and the radial profile of F_{cl} became flatter as the flow regime changed to the fast fluidization. That was because the solid-mass flux in the riser bed increased simultaneously.

In the splash zone (Figure 17a), similar radial profiles of F_{cl} for the transition and the fast fluidization flow regimes could also be observed. However, the radial profile of F_{cl} for the turbulent flow regime here was rather different from that observed in the dense bottom region. It showed a relatively lower value between r/R =0.4–0.8, with relatively higher values near the center and the bed wall regions. This profile might demonstrate that some clusters of FCC particles were injected from the dense bottom region into the splash zone by the eruption of gas void near the center of the bed, and returned to the lower dense bottom region through flowing downward near the bed wall. Thus, F_{cl} between r/R = 0.4–0.8 was lower than that near the center and the wall regions of the bed.

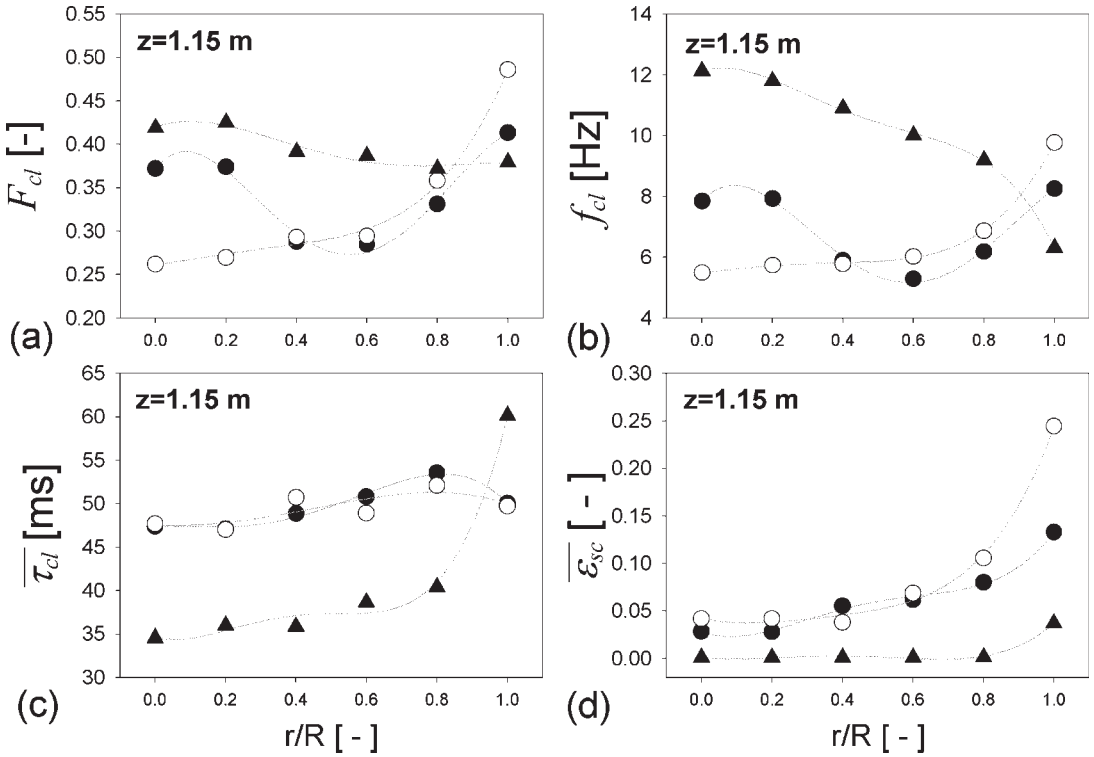

Figure 17. Radial distribution of dynamic properties of clusters in the splash zone (z = 1.15 m).

(●: U_g = 0.91 m/s, G_s = 0 kg/m^{2}s; ○: U_g =1.45 m/s, G_s = 1.14 kg/m^{2}s; ▲: U_g = 1.86 m/s, G_s = 19.5 kg/m^{2}s).

Cluster frequency f_{cl}

For the turbulent flow regime, f_{cl} in the dense bottom region increased slightly from the bed center toward the bed wall, while a sharp increase was observed near the bed-wall region (r/R $\cong$ 1) as shown in Figure 16b. It was ascribed to the significant wall effect near the bed wall that caused the solid particles agitate violently there, thus, a relatively higher f_{cl} was obtained. In the splash zone, as shown in Figure 17b, f_{cl} revealed a similar radial profile as F_{cl} in Figure 17a due to the motion of FCC particles discussed in the last paragraph. For the transition flow regime, f_{cl} at the core region was lower both in the dense bottom region and the splash zone. Comparing f_{cl} in Figures 16b and 17b, the value of f_{cl} is observed to increase with increasing axial elevation. This result implied that clusters were gradually accelerated from the dense bottom region to the splash zone, thus, a larger amount of clusters per sampling period was obtained at a higher elevation. For the fast fluidization flow regime, f_{cl} between r/R = 0–0.8 in the splash zone was apparently higher than that in the dense bottom region; on the contrary, f_{cl} near the bed wall (r/R $\cong$ 1) in the splash zone was obviously lower than that in the dense bottom region. This could be ascribed to the fact that the intensive solids acceleration at the core region quickly injected the particle clusters upward from the dense bottom region to the splash zone, and reduced the cluster size. Hence, a relatively higher f_{cl} was found between r/R = 0–0.8. Meanwhile, a part of the particle clusters in the splash zone moved transversely from the core region to the bed wall, and then flowed downward with enlarging its size. Therefore, fewer clusters per sampling period (equivalent to lower f_{cl}) were obtained near the bed wall.

Average cluster duration time $\overline{\tau_{cl}}$

In Figure 16c, $\overline{\tau_{cl}}$ near the center of the bed (r/R = 0–0.4) apparently became lower with increasing U_g. However, the radial profile of $\overline{\tau_{cl}}$ at 0.4 < r/R < 1 was rather complex. Since $\overline{\tau_{cl}}$ was dependent on both the cluster vertical length and velocity, e.g., a long $\overline{\tau_{cl}}$ might represent a long length of cluster or a cluster with slow velocity near the tip of the probe, and vice-versa. It was difficult to characterize which parameter contributed the more significant effect on $\overline{\tau_{cl}}$ in this region. In the splash zone (Figure 17c), the radial profile of $\overline{\tau_{cl}}$ in the turbulent flow regime was quite similar to that in the transition flow regime due to the approximate range of the local average solids holdup $\overline{\varepsilon_s}$ in both flow regimes ($\overline{\varepsilon_s}$ = 0.019−0.082 for the turbulent flow regime; $\overline{\varepsilon_s}$ = 0.02−0.18 for the transition flow regime). This result was also confirmed by Manyele et al.[9] who demonstrated that $\overline{\tau_{cl}}$ is positively dependent on $\overline{\varepsilon_s}$. In the fast fluidization flow regime, a smaller $\overline{\tau_{cl}}$, generally responding to a higher f_{cl}, was obtained at the core region (r/R = 0–0.8); on the other hand, a larger $\overline{\tau_{cl}}$ responding to a lower f_{cl}, was clearly observed near the bed wall (r/R $\cong$ 1). Therefore, the radial profile of $\overline{\tau_{cl}}$ in the splash zone revealed a typical core-annulus flow structure in the fast fluidization flow regime. A more clear description of the cluster structure would be obtained by combining the radial distribution of cluster velocity and $\overline{\tau_{cl}}$.

Local average solids holdup in clusters $\overline{\varepsilon_{sc}}$

The radial distribution of the local average solids holdup in clusters $\overline{\varepsilon_{sc}}$ showed a smooth increase from the bed center toward the bed wall in the turbulent fluidization regime

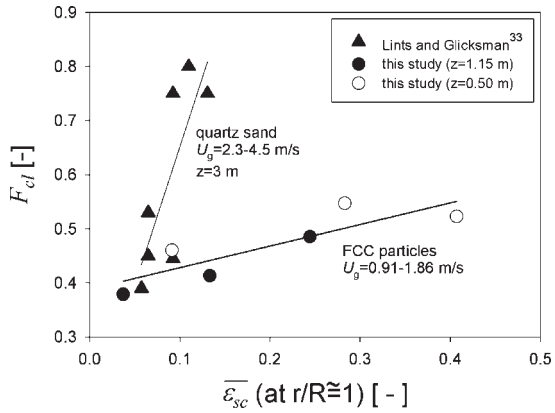

Figure 18. Appearance time fraction of clusters vs. average solids holdup in clusters near the bed wall region.

Lints and Glicksman[33] defined a cluster as any group of five or more sequential particle strikes with 2 ms maximum time between any two sequential strikes. $\overline{\varepsilon_{sc}}$ was calculated by the square root of cross-sectional average solids fraction in their study.

(U_g = 0.91 m/s) in both the dense bottom region and the splash zone. While $\overline{\varepsilon_{sc}}$ in the splash zone was apparently smaller than that in the dense bottom region (Figures 16d and 17d). It revealed that most of the FCC particles were kept in the dense bottom region of the riser in the turbulent fluidization flow regime. As the superficial gas velocity increased (U_g = 1.45 m/s), $\overline{\varepsilon_{sc}}$ in the dense bottom region came to a dramatically lower value as compared to the turbulent flow regime due to significant entrainment of solid particles. However, in the splash zone $\overline{\varepsilon_{sc}}$ did not change apparently within the core region of $0 \leq r/R \leq 0.6$. $\overline{\varepsilon_{sc}}$ near the bed wall ($r/R > 0.6$) increased obviously owing to the increasing amount of particle clusters/swarms moving downward there. When further increasing the gas velocity (U_g = 1.86 m/s), a core-annulus structure, characterized by the flat radial profile of $\overline{\varepsilon_{sc}}$ in the core region ($0 \leq r/R \leq 0.8$), and the sharp increase of $\overline{\varepsilon_{sc}}$ near the bed wall ($0.8 < r/R \leq 1.0$), was clearly observed both in the dense bottom region and in the splash zone.

Cluster dynamic properties near the bed wall region

Numerous efforts on characterization of cluster dynamic properties in previous studies[33–38] have focused on the near-wall region of CFBs, and the formation of clusters in this region have always played an important role on the bed-to-wall heat transfer and erosion. Since the solids holdup $\overline{\varepsilon_{sc}}$, and appearance time fraction of clusters F_{cl}, had a substantial effect on these phenomena, they are quantitatively discussed in this section.

Figure 18 shows the dependency of F_{cl} on the average cluster solids holdup $\overline{\varepsilon_{sc}}$ near the bed-wall region. Apparently F_{cl} increased with increasing $\overline{\varepsilon_{sc}}$ in both the splash zone and the dense bottom region of the riser bed. The data Lints and Glicksman[33] obtained using the particle impact probe also clearly revealed F_{cl} increased with increasing $\overline{\varepsilon_{sc}}$ for quartz sand particles. This result implied that the increase of F_{cl} equated to increase the wall coverage fraction of particles, leading to the stronger particle-particle interaction near the bed wall. The enhanced particle-particle interaction caused the particles in clusters to aggregate more tightly. Consequently, $\overline{\varepsilon_{sc}}$ near the bed wall increased. Besides, the slope of Lints and Glicksman's[33] data in Figure 18 was much sharper than that in this study. The exact reason is not yet clear; however, it might be ascribed to the use of different kinds of particles.

Increasing the cross-sectional average solids holdup $<\overline{\varepsilon_s}>$ also increased F_{cl} near the bed wall region for the dense bottom region or the splash zone. This result had been confirmed by previous studies[33,34,35] as shown in Figure 19. Again, different slopes of data for different studies were observed in this figure. It revealed that the slope might

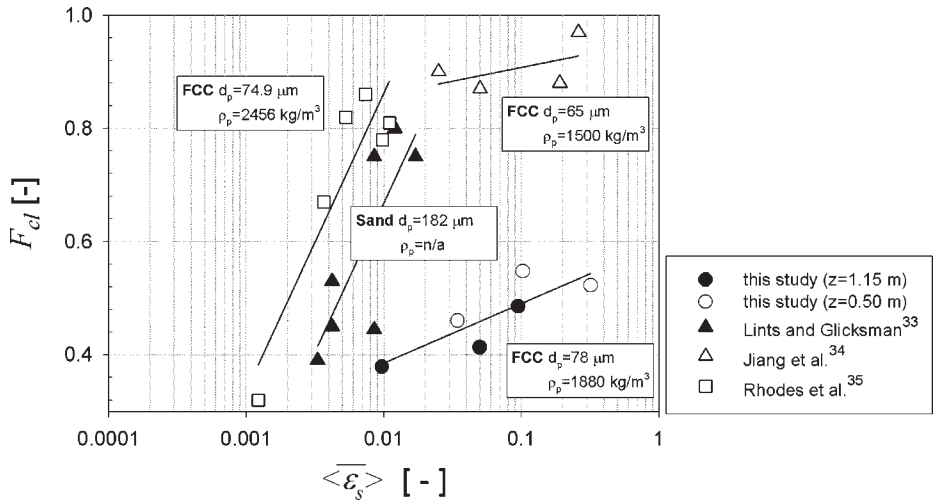

Figure 19. Appearance time fraction of clusters near the bed wall region vs. the cross-sectional average solids holdup.

The operation conditions are, U_g = 2.3–4.5 m/s, G_s not mentioned for Lints and Glicksman[33]; U_g = 2.1 m/s, G_s = 40 kg/m^{2}s for Jiang et al.[34]; U_g = 2-3 m/s, G_s = 8–60 kg/m^{2}s for Rhodes et al.[35]

depend on the particle density; namely, the higher density the particles had, the larger the slope was. However, there was not enough data to address any further conclusion. To verify the relationship between the slope and particle density, further study should be done.

Figure 20 shows the relationship between the local average solids holdup in clusters $\overline{\varepsilon_{sc}}$ near the bed wall region, and the cross-sectional average solids holdup $<\overline{\varepsilon_s}>$. The data by Lin et al.,[30] Lints and Glicksman,[33] Gidaspow et al.[36] and Horio et al.[37] are also plotted in this figure for comparison. It was observed that $\overline{\varepsilon_{sc}}$ increased apparently with increasing $<\overline{\varepsilon_s}>$, and the data in this study revealed the similar trend as that reported in literatures. This result was also consistent with Harris et al.'s[38] study. They proposed that $\overline{\varepsilon_{sc}}$ near the bed-wall region is a function of $<\overline{\varepsilon_s}>$, rather than an uniform solids holdup profile.[39]

The particle clusters were not only observed near the bed-wall region, but also in the core region of CFBs.[7,30,40,41] As shown in Figures 16d and 17d, $\overline{\varepsilon_{sc}}$ was relatively smaller in the core region, and increased toward the bed wall. This trend was smoother in the turbulent flow regime, while it was rather sharp near the bed wall region in the transition and the fast fluidization flow regimes. Similar profiles were also reported by Manyele et al.[9] For FCC particles in the freeboard region (z = 6.34 m), they found the radial profiles of $\overline{\varepsilon_{sc}}$, are quite similar to that of the local average solids holdup $\overline{\varepsilon_s}$. Based on PDPA measurements, Liu et al.[13] found that the voidage/solids holdup inside clusters seems to be a function of $\overline{\varepsilon_s}$ in bubbling and turbulent fluidized beds. In this study, the variation of $\overline{\varepsilon_{sc}}$ at different radial positions, including in the core and near the bed wall regions, with the corresponding $\overline{\varepsilon_s}$ was also investigated. Figure 21 shows that there was a positive relationship between $\overline{\varepsilon_{sc}}$ and $\overline{\varepsilon_s}$. The experimental data could be fitted quite well with a sigmoid formula as follows

$$\overline{\varepsilon_{sc}} = \frac{0.595\overline{\varepsilon_s}^{1.143}}{0.165 + \overline{\varepsilon_s}^{1.143}} \tag{16}$$

The square of correlation coefficient of curve fitting is 0.981 for $\overline{\varepsilon_s}$, ranging from 0.4 to 8.0 $\times$ 10^{-4}. Figure 21 also reveals that no matter in the splash zone or in the dense bottom region, $\overline{\varepsilon_{sc}}$ could be predicted well by Eq. 16.

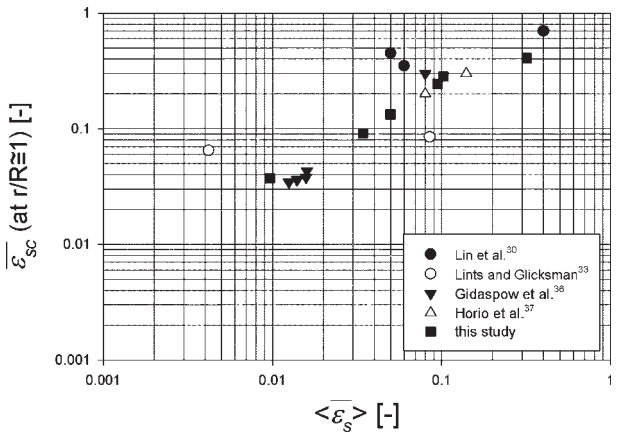

Figure 20. Average solids holdup in clusters near the bed wall region vs. the cross-sectional average solids holdup.

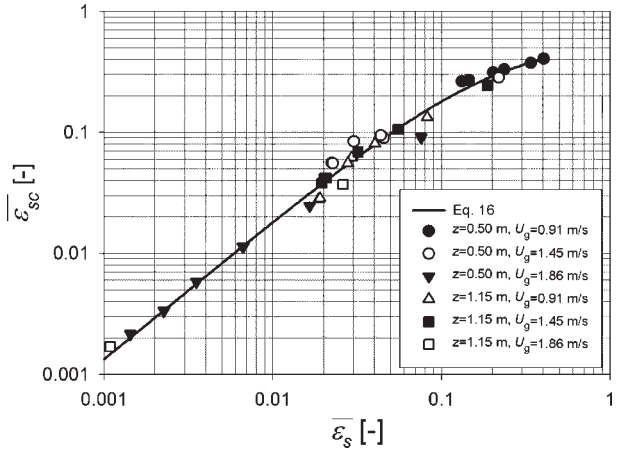

Figure 21. Average solids holdup in clusters vs. the local average solids holdup.

Conclusions

By multiresolution analysis of wavelet transform on the transient solids holdup fluctuation signals, a wavelet-threshold criterion was developed to distinguish the cluster phase and the void phase from the measurements in the splash zone, and the dense bottom region in a circulating fluidized bed. Significant results of this study were summarized as follows:

- The values of cluster dynamic properties obviously depended on the approximation subsignal of different levels. After considering most of experimental conditions in this study, the approximation subsignal A_{11} was specified as the threshold. It not only successfully identified the particle clusters phase, but also tracked the time-variant features of the original solids holdup fluctuation signals.
- PDF of solids holdup in the cluster phase revealed a unimodal distribution in the dense bottom region of the riser bed. It gradually skewed from the lefthand side to the right-hand side as the flow regime changed from turbulent to fast fluidization.
- The radial distribution of cluster dynamic properties in the dense bottom region was rather complex in comparison with that in the dilute freeboard region as shown in literature,[10,12,33,35,40] while the core-annulus flow pattern also was observed in the splash zone at higher gas velocity.
- Near the bed-wall region (r/R $\cong$ 1), both F_{cl} and $\overline{\varepsilon_{sc}}$ increased with increasing $<\overline{\varepsilon_s}>$. At different radial positions, including in the core and near the bed wall regions $\overline{\varepsilon_{sc}}$, could be simply expressed as a function of $\overline{\varepsilon_s}$ and predicted well by Eq. 16.

Notation

$a_{J,k}$ = approximation coefficient of level J
A_J(t) = approximation subsignal of level J
APF = absolute pressure fluctuations, Pa
$d_{j,k}$ = detail coefficient of level j
d_p = mean particle size, μm
D_j(t) = detail signal of level j
E = energy of original signal
E_J^A = energy of approximation signal of level J
E_j^D = energy of detail signal of level j

f_{cl} = cluster frequency, s^{-1}
f_s = sampling frequency, s^{-1}
F_{cl} = appearance time fraction of clusters
G_s = solid mass flux, kg $m^{-2}s^{-1}$
$G_{s,max}$ = maximum solid mass flux, kg $m^{-2}s^{-1}$
H_s = static bed height, m
I = integer
I_0 = intensity of light in empty bed, volt
I_1 = intensity of measured reflective light at any condition, volt
I_{max} = intensity of reflective light in loosely packed bed, volt
$\bar{I}$ = normalized intensity of measured reflective light at any condition, volt
m = mass of FCC particles trapped in the shutter valve, kg
n = the coefficient of σ_s
n_{cl} = total number of clusters in a sampling period
N = number of data points
PDF = probability density function
r = radial distance from the centerline of riser bed, m
R = radius of riser bed, m
r/R = relative radial position
R^2 = square of correlation coefficient
S = cross-sectional area of test pipe for calibration of probe, m^2
t = time, s
t_a = the time at which the ε_s increases beyond the threshold, s
t_b = the time at which the ε_s decreases below the threshold, s
T = total sampling time, s
U_c = transition velocity at which the standard deviation of pressure fluctuations reaches a maximum, m s^{-1}
U_g = superficial gas velocity in the riser, m s^{-1}
U_k = superficial gas velocity corresponding to the leveling-off standard deviation of pressure fluctuations as U_g increases, m s^{-1}
U_{se} = onset velocity of significant solids entrainment, m s^{-1}
U_{tr} = transport gas velocity, m s^{-1}
$x(t)$ = time series signal
z = axial position of probe above the gas distributor, m

Greek letters

ΔL = length between the two slide plates of shutter valve, m
ε_s = transient solids holdup
$<\bar{\varepsilon_s}>$ = cross sectional average solids, holdup
$\bar{\varepsilon_s}$ = local average solids holdup
$\bar{\varepsilon_{sc}}$ = local average solids holdup in clusters
$\bar{\varepsilon}_{sc,\,i}$ = local average solids holdup in the ith cluster
ϕ = father wavelet function
$\phi_{j,k}(t)$ = dilated father wavelet
ρ_p = particle density, kg m^{-3}
ψ = mother wavelet function
$\psi_{j,k}(t)$ = dilated mother wavelet
σ_{APF} = standard deviation of absolute pressure fluctuations, Pa
σ_s = standard deviation of solids holdup fluctuation signal
$\bar{\tau}_{cl}$ = averaged cluster duration time, s
τ_i = duration time of the ith cluster identified, s

Subscripts

i = index
j = decomposition level of MRA
J = the maximum decomposition level of MRA
k = time shift

Literature Cited

1. Chen JC. Clusters. *AIChE Symp Ser*. 1996;92(313):1–5.
2. Horio M, Ishii H, Nishimuro M. On the nature of turbulent and fast fluidized beds. *Powder Technol*. 1992;70:229–236.
3. Horio M, Clift R. A note on terminology: 'cluster' and 'agglomerates'. *Powder Technol*. 1992;70:196.
4. Helland E, Occelli R, Tadrist L. Computational study of fluctuating motions and cluster structures in gas-solid flows. *Int J Multiphase Flow*. 2002;28:199–223.
5. Ito M, Tsukada M, Shinamura J, Horio M. Prediction of cluster size and slip velocity in circulating fluidized beds by a DSMC model. In: Fan LS, Knowlton TM, eds. *Fluidization IX*. New York: Engineering Foundation; 1998:525–532.
6. Ouyang J, Li J. Discrete simulations of heterogeneous structure and dynamic behavior in gas-solid fluidization. *Chem Eng Sci*. 1999;54:5427–5440.
7. Wang S, Liu H, Lu H, Liu W, Ding J, Li W. Flow behavior of clusters in a riser simulated by direct simulation Monte Carlo method. *Chem Eng J*. 2005;106:197–211.
8. Rudnick C, Werther J. The discrimination of cluster characteristics from fiber optic probe signals in circulating fluidized beds. In: Fan LS, Knowlton TM, eds. *Fluidization IX*. New York: Engineering Foundation; 1998:573–580.
9. Manyele SV, Parssinen JH, Zhu J-X. Characterizing particle aggregates in a high-density and high-flux CFB riser. *Chem Eng J*. 2002;88:151–161.
10. Soong CH, Tuzla K, Chen JC. Identification of particle clusters in circulating fluidized bed. In: Avidan AA, ed. *Circulating Fluidized Bed Technology IV*. New York: AIChE; 1994:615–620.
11. Tuzla K, Sharma AK, Chen JC, Schiewe T, Wirth KE, Molerus O. Transient dynamics of solid concentration in downer fluidized bed. *Powder Technol*. 1998;100:166–172.
12. Sharma AK, Tuzla K, Matsen J, Chen JC. Parametric effects of particle size and gas velocity on cluster characteristics in fast fluidized beds. *Powder Technol*. 2000;111:114–122.
13. Liu XH, Gao SQ, Li JH. Characterizing particle clustering behavior by PDPA measurement for dilute gas-solid flow. *Chem Eng J*. 2005;108:193–202.
14. Guenther C, Breault R. Wavelet analysis to characterize cluster dynamics in a circulating fluidized bed. *Powder Technol*. 2007;173:163–173.
15. Zijerveld RC, Johnsson F, Marzocchella A, Schouten JC, van den Bleek CM. Fluidization regimes and transition from fixed bed to dilute transport flow. *Powder Technol*. 1998;95:185–204.
16. Schouten JC, Zijerveld RC, van den Bleek CM. Scale-up of bottom-bed dynamics and axial solids-distribution in circulating fluidized beds of Geldart-B particles. *Chem Eng Sci*. 1999;54:2103–2112.
17. Ji H, Ohara H, Kuramoto K, Tsutsumi A, Yoshida K, Hirama T. Nonlinear dynamics of gas-solid circulating fluidized-bed system. *Chem Eng Sci*. 2000;55:403–410.
18. Ren J, Li J. Wavelet analysis of dynamic behavior in fluidized beds. In: Fan LS, Knowlton TM, eds. *Fluidization IX*. New York: Engineering Foundation; 1998:629–636.
19. Ren J, Mao Q, Li J, Lin W. Wavelet analysis of dynamic behavior in fluidized beds. *Chem Eng Sci*. 2001;56:981–988.
20. Ellis N, Briens LA, Grace JR, Bi HT, Lim CJ. Characterization of dynamic behaviour in gas-solid turbulent fluidized bed using chaos and wavelet analyses. *Chem Eng J*. 2003;96:105–116.
21. Lu X, Li S, Du L, Yao J, Lin W, Li H. Flow structures in the downer circulating fluidized bed. *Chem Eng J*. 2005;112:23–31.
22. Shou MC, Leu LP. Energy of power spectral density function and wavelet analysis of absolute pressure fluctuation measurements in fluidized beds. *Trans IChemE, Part A, Chem Eng Res Des*. 2005;83:478–491.
23. Wen CY, Yu YH. A generalized method for predicting the minimum fluidization velocity. *AIChE J*. 1996;12:610–612.
24. Schnitzlein MG, Weinstein H. Flow characterization in high-velocity fluidized beds using pressure fluctuations. *Chem Eng Sci*. 1988;43:2605–2614.
25. Bi HT, Grace JR, Zhu JX. Regime transitions affecting gas-solids suspensions and fluidized beds. *Trans IChemE, Part A, Chem Eng Res Des*. 1995;73:154–161.
26. Ishida M, Tanaka H. An optical probe to detect both bubbles and suspended particles in a three-phase fluidized bed. *J Chem Eng Jpn*. 1982;15(5):389–391.
27. Zhang H, Johnston PM, Zhu JX, de Lasa HI, Bergougnou MA. A novel calibration procedure for a fiber optic solids concentration probe. *Powder Technol*. 1998;100:260–272.
28. Herbert PM, Gauthier TA, Briens CL, Bergougnou MA. Application of fiber optic reflection probes to the measurement of local particle velocity and concentration in gas-solid flow. *Powder Technol*. 1994;80:243–252.
29. Mallat S. A theory for multiresolution signal decomposition: the wavelet representation. *IEEE Trans Pattern Anal Mach Intell*. 1989;11(7):674–693.
30. Lin Q, Wei F, Jin Y. Transient density signal analysis and two-phase microstructure flow in gas-solid fluidization. *Chem Eng Sci*. 2001;56:2179–2189.

31. Taxil I, Guigon P, Archimbault F, Gauthier TA. Gas flow characterization in turbulent fluidization for FCC catalyst. In: Fan LS, Knowlton TM, eds. *Fluidization IX*. New York: Engineering Foundation; 1998:69–76.
32. Shou MC. *The study of the existence of transition velocities and the hydrodynamics of turbulent fluidized beds*. National Taiwan University, Taipei, Taiwan; 2004. Ph.D. dissertation.
33. Lints MC, Glicksman LR. The structure of particle clusters near the wall of a circulating fluidized bed. *AIChE Symp Ser*. 1993; 89(296):35–52.
34. Jiang P, Cai P, Fan LS. Transient flow behavior in fast fluidization. In: Avidan AA, ed. *Circulating Fluidized Bed Technology IV*. New York: AIChE; 1994:111–116.
35. Rhodes M, Mineo H, Hirama T. Particle motion at the wall of a circulating fluidized bed. *Powder Technol*. 1992;70:207–214.
36. Gidaspow D, Tsuo YP, Luo KM. Computed and experimental cluster formation and velocity profiles in circulating fluidized beds. In: Grace JR, Shemilt LW, Bergougnou MA, eds. *Fluidization VI*. New York: AIChE; 1989:81–88.
37. Horio M, Morishita K, Tachibana O, Murata N. Solid distribution and movement in circulating fluidized bed. In: Basu P, Large JF, eds. *Circulating Fluidized Bed Technology II*. Toronto: Pergamon Press; 1988:147–154.
38. Harris AT, Davidson JF, Thorpe RB. The prediction of particle cluster properties in the near wall region of a vertical riser. *Powder Technol*. 2002;127:128–143.
39. Yerushalmi J, Cankurt NT, Geldart D, Liss B. Flow regimes in vertical gas-solid contact systems. *AIChE Symp Ser*. 1976;74(176):1–13.
40. Wei F, Jin Y, Yu Z. The visualization of macro structure of the gas-solids suspension in high density CFB. In: Avidan AA, ed. *Circulating Fluidized Bed Technology IV*. New York: AIChE; 1994:588–593.
41. Takeuchi H, Pyatenko AT, Hatano H. Gross behavior of parabolic strands in a riser. In: Fan LS, Knowlton TM, eds. *Fluidization IX*. New York: Engineering Foundation; 1998:173–180.

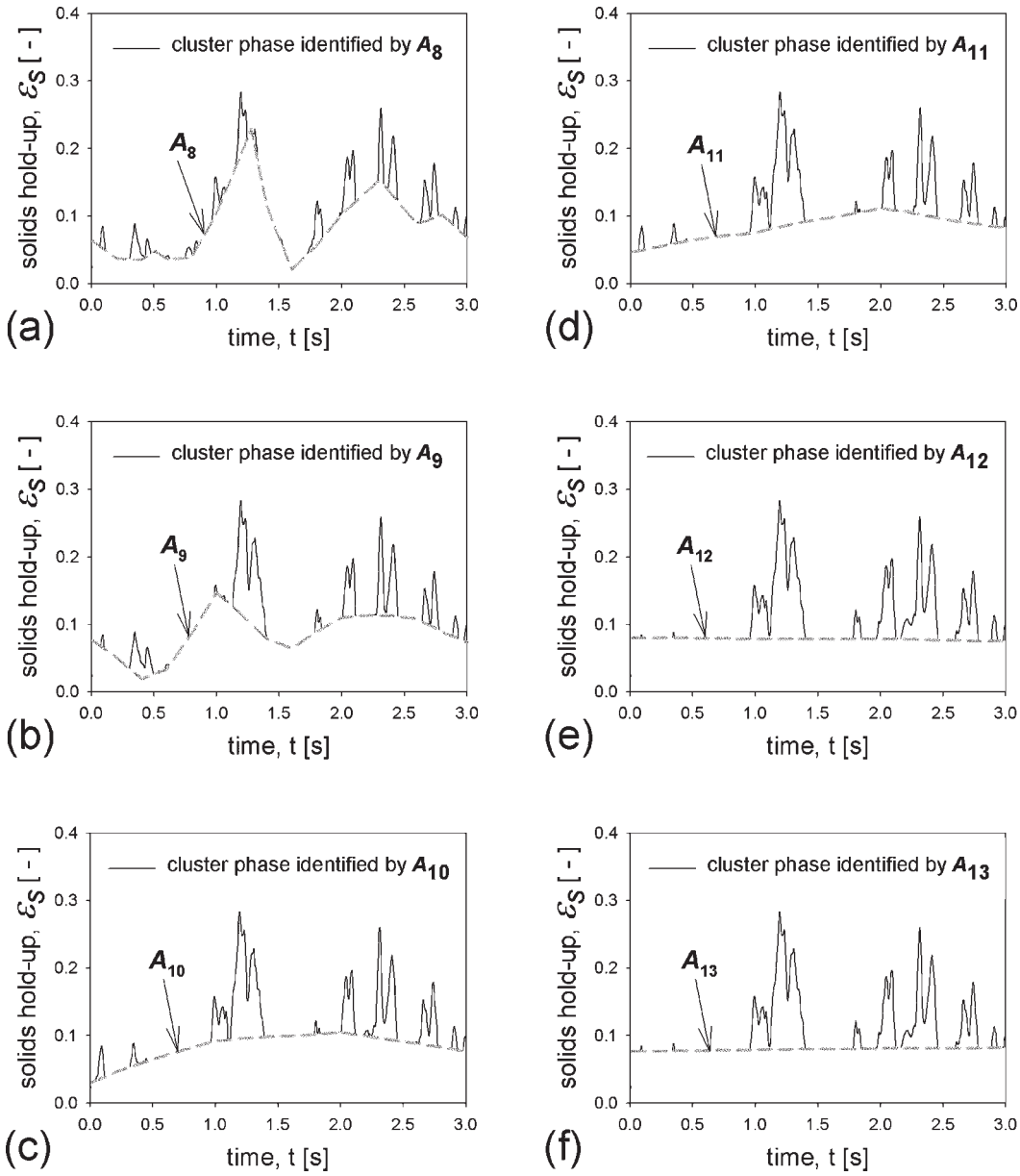

Figure A1. Cluster identification by different levels of approximation subsignals (a) A_8, (b) A_9, (c) A_{10}, (d) A_{11}, (e) A_{12} and (f) A_{13}.

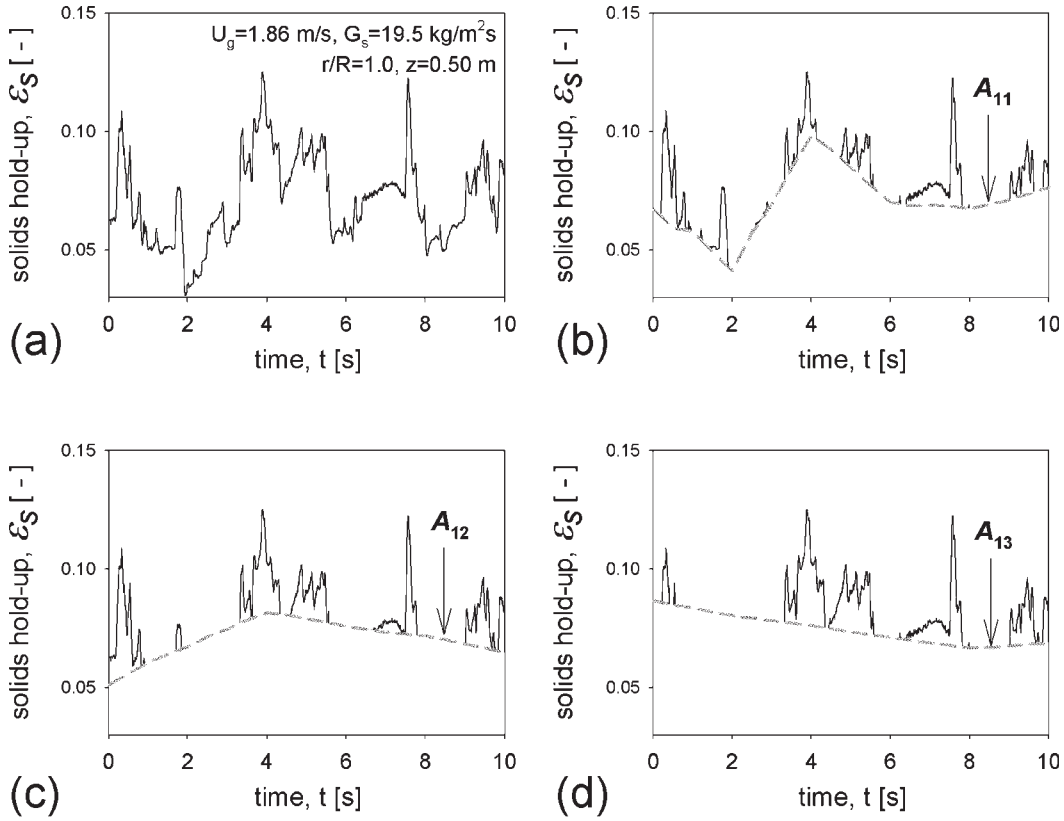

Figure A2. Comparison of cluster identification by A_{11}, A_{12} and A_{13} in the dense bottom region.

Appendix: Comparison of Cluster Identification by Different Levels of Approximation Subsignals

Figure A1 shows the solids holdup fluctuations of cluster phase (represented by the solid line) identified by different levels of approximation subsignals (represented by the dashed line). In Figure A1a, the approximation subsignal A_8 between $t = 0.75$ and 1.6 s almost covered up the original solids holdup fluctuation signal in this time interval, so that only small peaks of cluster phase could be identified. With an increase in the level, the approximation subsignal became more and more smooth, and the larger peaks gradually protruded beyond the threshold line, as shown in the time interval $t = 1$–1.5 s in Figure A1b and c. When further increasing the level beyond 10, the difference among the cluster phase identified by different levels of approximation subsignals gradually reduced, as shown in Figure A1d–f.

However, if the original solids holdup fluctuation signals exhibited considerably violent oscillations, especially in the dense bottom region, some peaks of cluster phase might not be identified by the approximation subsignals with too large a level. Figure A2 shows the cluster identification by A_{11}, A_{12} and A_{13} in the dense bottom region. The result showed that with increased the level of threshold from 11 to 13, a clear peak at about $t = 1.8$ s gradually reduced its height (Figure A2c) and eventually disappeared (Figure A2d). It might be ascribed to that A_{12} and A_{13} were too smooth to characterize the global time-variant feature of the original solids holdup fluctuation signal.

Manuscript received May 9, 2008, and revision received Oct. 14, 2008.